



OPEN

## Influence of rock stratification on the performance of tailored wetting agents in open pit coal mines

Xiaoliang Zhao<sup>1</sup>✉, Zhaolin Shen<sup>1</sup>, Bandna Bharti<sup>2</sup>, Fangwei Han<sup>3</sup> & Shaohui Feng<sup>1</sup>

Dust control through water injection and pre-wetting effectively reduces dust pollution at opencast coal mines by targeting its source. The wetting effect of a single wetting agent is limited for different Bedded Igneous Rocks in the Dananhu coal mine in Xinjiang. The study focused on identifying suitable surfactants by performing monomer preference experiments. A range of surfactants were evaluated to explore their degree of wetting in six distinct rock layers. Key performance indicators such as surface tension and wetting time were analyzed, and orthogonal experiments determined the optimal concentrations of the water wetting agent: 0.15% OP, 0.10% Fast T, 0.15% LAD-40, and 0.10% LAB-35. Comparative performance tests revealed that the developed wetting agent outperformed three commercially available wetting agents in terms of wetting efficiency. Using FLUENT, a three-dimensional flow field model for water injection and pre-wetting was established to evaluate the effects of water injection composition and pressure on pre-wetting performance. Experimental validation showed strong agreement with simulation results, highlighting the influence of injection parameters on wetting efficiency. This study provided a practical solution to address the challenge of uneven wetting in stratified raw rock, offering innovative advancements in dust control for surface coal mine working faces.

**Keywords** Opencast coal mines, Bedded igneous rocks, Water-injected wetting agents, Orthogonal experiments, Numerical simulations

Dust generation in opencast coal mining is predominantly attributed to activities such as drilling, blasting, excavation, loading, transportation, discharge, and material reclamation, with the working face being a major source<sup>1,2</sup>. Drilling and blasting are recognized as the most significant contributors to particulate emissions across various size ranges<sup>3,4</sup>. According to 2023 statistics, China's energy production and consumption reached 5.72 billion tonnes of standard coal<sup>5,6</sup>.

The cumulative geological reserves in Xinjiang and Inner Mongolia constituted 95.56% of the nation's surface coal mine reserves, while their recoverable reserves accounted for 95.41% of the total recoverable reserves<sup>7</sup>. These regions are predominantly water-scarce, and the stripping of rock and soil materials at the working face often results in dry conditions that facilitate significant dust production<sup>8–10</sup>. Many dust particles generated in surface coal mines are less than 10 microns in diameter<sup>11,12</sup>. Particles of this size are primarily deposited in the respiratory tract, while those smaller than 5 microns can penetrate deeper into the lungs, leading to respiratory diseases and pulmonary heart conditions<sup>13–15</sup>. Additionally, dust accelerates the wear and tear of machinery components in open-pit mining operations, increasing maintenance costs, and reducing operational efficiency<sup>16</sup>. Dust exposure also negatively impacts worker productivity and health, further exacerbating the challenges of dust management in these mining environments<sup>17,18</sup>.

Dust suppression is currently one of the most effective strategies for reducing dust pollution in surface coal mines<sup>19–21</sup>. Wetting agents, primarily composed of surfactants, significantly reduce surface tension and wetting time of solutions, thereby enhancing their dust suppression efficiency. Patrakov et al. have investigated the physical and chemical properties of coal, revealing that coal hydrophobicity was strongly associated with its carbon-to-oxygen ratio<sup>22</sup>. S.A. Silvester, Tang et al. utilized numerical simulation tools to model and analyze the dispersion dynamics of blasting dust in surface coal mines under wind influence and examined the behavior

<sup>1</sup>Environmental Science and Engineering Department, Liaoning Technical University, Fuxin 123000, China.

<sup>2</sup>Department of Chemistry, DAV University, Jalandhar, Punjab, India. <sup>3</sup>College of Safety Science and Engineering, Liaoning Technical University, Huludao City 125105, Liaoning Province, China. ✉email: zhaoxiaoliang@lntu.edu.cn

of dust particles with varying characteristics<sup>23,24</sup>. Weimin Cheng, Ping Chang, and Lu Zhao et al. explored the effects of combining different surfactants, demonstrating that optimal wetting behavior of coal dust varied significantly with the mass fractions of compound solutions<sup>25–27</sup>. Furthermore, the surface tension of solutions decreases markedly upon reaching the critical micelle concentration (CMC) of surfactants. Xiazhong Zheng, and Deji Jing conducted numerical simulations to study the spatial and temporal distribution of blasting dust concentrations<sup>28,29</sup>. They also examined the diffusion patterns of dust generated during drilling operations and the dispersion of dust during truck unloading in open-pit coal mines<sup>30,31</sup>. This study focuses on the high-temperature zones of the fire area in the Dananhu No. 2 open-pit coal mine, Xinjiang. The laminated structure of rocks in the fire area, coupled with distinct physicochemical properties across six distinct rock layers, poses challenges for pre-wetting with conventional wetting agents. To address these limitations, this paper develops a novel water-injection wetting agent designed to improve pre-wetting performance in stratified rock formations. The geological conditions of the Xinjiang Dananhu No. 2 open-pit coal mine present unique challenges for dust control and water injection strategies<sup>32,33</sup>. Firstly, spontaneous combustion in local coal seams occurred in the mine's early history, resulting in high-temperature sintering and the formation of a fire zone covering 7.06 km<sup>2</sup>, which constitutes one-third of the total stripping area. Additionally, the original rock is dry and hydrophobic, making it highly susceptible to dust generation. Secondly, the stratification characteristics of six distinct rock layers at the working face are distinct, with significant variations in physicochemical properties between six distinct rock layers. This heterogeneity reduces the effectiveness of conventional vertical sprinkling methods at the working face, resulting in poor pre-wetting for dust suppression and frequent water bypassing, which leads to liquid accumulation near the lower steps<sup>34–37</sup>.

This study examined the physical and chemical properties of the rock and soil at the Dananhu No. 2 mine. It included chemical group analysis and microscopic morphology. The aim was to investigate variations in hydrophilicity across different layers<sup>38–41</sup>. The wetting effects of four surfactants: anionic, cationic, amphoteric, and nonionic on the raw rock of six distinct rock layers were evaluated. This helped identify the primary components of the wetting agents. Orthogonal experiments were performed to optimize the formulation of water-injection wetting agents. Surface tension and wetting time were used as the main control indices<sup>42,43</sup>. The effectiveness of the water-injection wetting agents was compared to three commercially available agents to comprehensively assess their impact on the bedded raw rock's wetting properties. To further investigate the field performance of the selected water-injection wetting agent, numerical simulations using Fluent software were combined with experimental validation to model the penetration of water and wetting agents into the six distinct rock layers. Based on the results of these simulations and experiments, the optimal injection pressure for water-injection and pre-wetting of stratified raw rock was determined. Pressure penetration experiments were conducted to verify the accuracy of the numerical simulation. The findings of this research provide valuable insights for the development of effective dust control technologies and processes involving water-injection and pre-wetting of bedded raw rock in open-pit coal mine operations<sup>44</sup>.

## Materials and experiments

### Collection and preparation of raw rock samples

In this study, raw rock samples were collected from the +475-working face of the second mine within the fire zone of Dananhu, Xinjiang. The rock strata were categorized into six distinct rock layers based on color: the upper yellow layer, pure red layer, yellow and white layer, middle layer, pure black layer, and lower layer, as shown in Fig. 1. Sampling was conducted from each of six distinct rock layers, and the sampling locations were indicated in Fig. 2, situated at coordinates 41°50'–42°15' N latitude and 94°10'–94°37' E longitude. A portion of the collected rock samples was initially crushed using a PE-400×600 jaw crusher. Equal amount from each layer of six distinct rock layers were combined and subsequently ground using an MQ750×1060 drum-type ball mill for 8 h. The resulting rock powder was then placed in a vacuum drying oven at 25 °C until a constant weight was achieved, at which point it was ready for further analysis. Additionally, larger rock samples were core drilled, cut, and polished to prepare cylindrical specimens with a height of 100 mm and a diameter of 50 mm for use in the pressure penetration tests<sup>45</sup>.

### Materials and equipment's

The primary materials utilized in the experimental procedures included various surfactants and chemical agents: dodecyldimethylbenzylammonium chloride (1227), cetyltrimethylammonium chloride (1631), sodium aliphatic alcohol polyvinyl chloride ether sulfate (AES), sodium dodecyl sulfate (SDS), sodium dodecylbenzenesulfonate (LAS-30), sodium dioctyl succinate sulfonate (Fast T), sodium  $\alpha$ -alkenylsulfonate (AOS), sodium sec-alkylsulfonate (SAS-60), polyethylene glycol 2000 (PEG2000), Tween-80, OP emulsifier, cocoamidopropyl betaine (CAB-35), lauryl amphoteric imidazoline (LAD-40), lauryl amideopropyl amine oxide (LAO-30), lauramidopropyl betaine (LAB-35), and potassium bromide (KBr). Pyroxene samples were obtained from the second mine in the Dananhu pyroxene region, Xinjiang.

The experimental equipment included a Fourier transform Infrared Spectrometer (GXIV5.0.1), a Field Emission Scanning Electron Microscope (FEI Quanta FEG 250), an Electrothermal Constant-Temperature Drying Oven (LDO-101-0), a Tablet Press (HY-12), a Contact Angle Measuring Instrument (SCI3000), an Electronic Balance (PTX-FA210), a fully Automated Tensiometer (JK99C), a Jaw Crusher (PE-400×600), a Drum-Type Ball Mill (MQ750×1060), and a Rock Full-Stress Multi-Field Coupled Triaxial Tester (ROCK 600–50).as illustrated in Fig. 3.

### Preparation of wetting solution

To prepare the wetting solution, surfactants such as OP emulsifier, Fast T, LAD-40, and LAB-35 A were measured according to the optimal ratio and added to a beaker along with 50 mL of water. The mixture was stirred at a

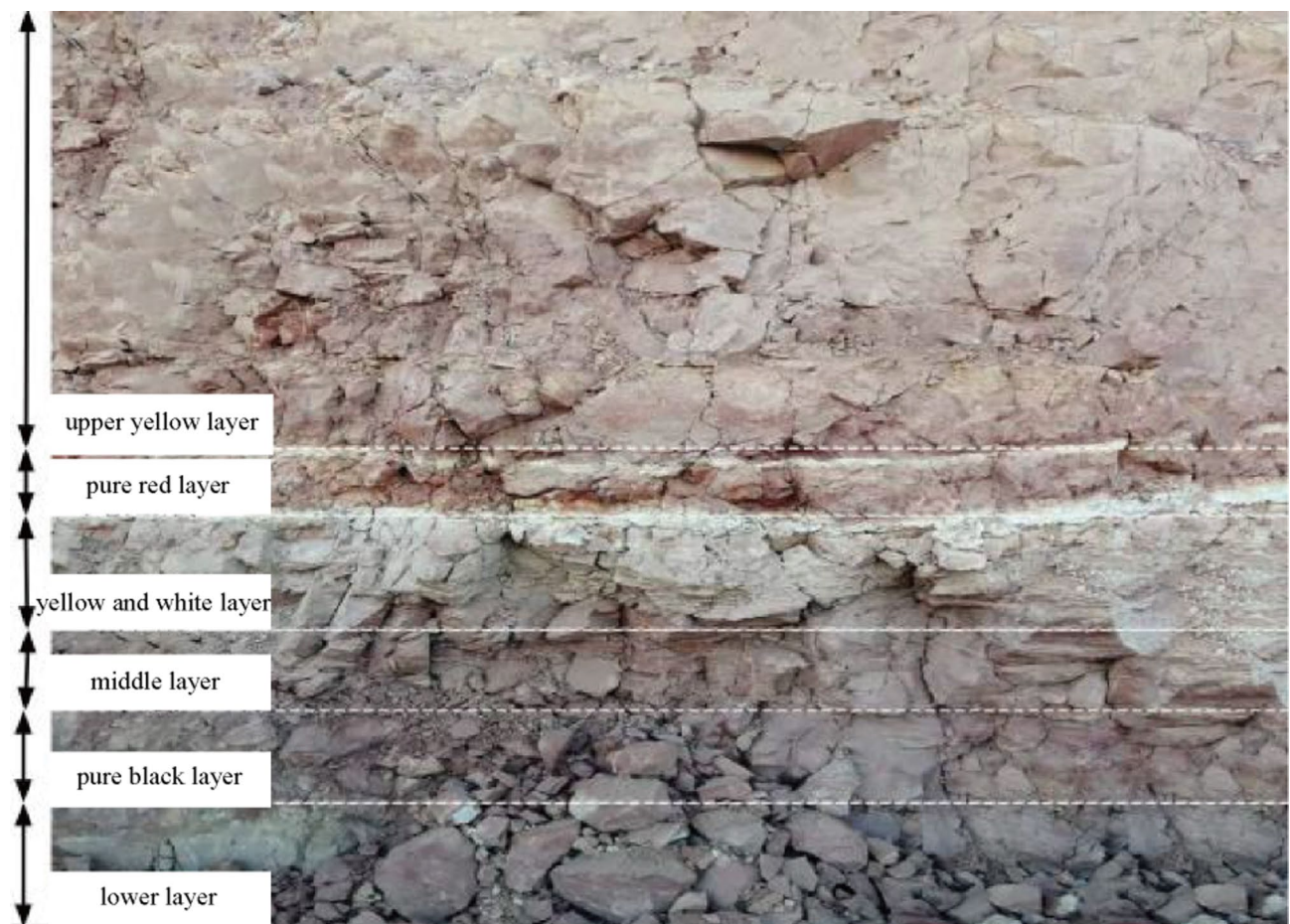


**Fig. 1.** The stratified structure of the raw rock.

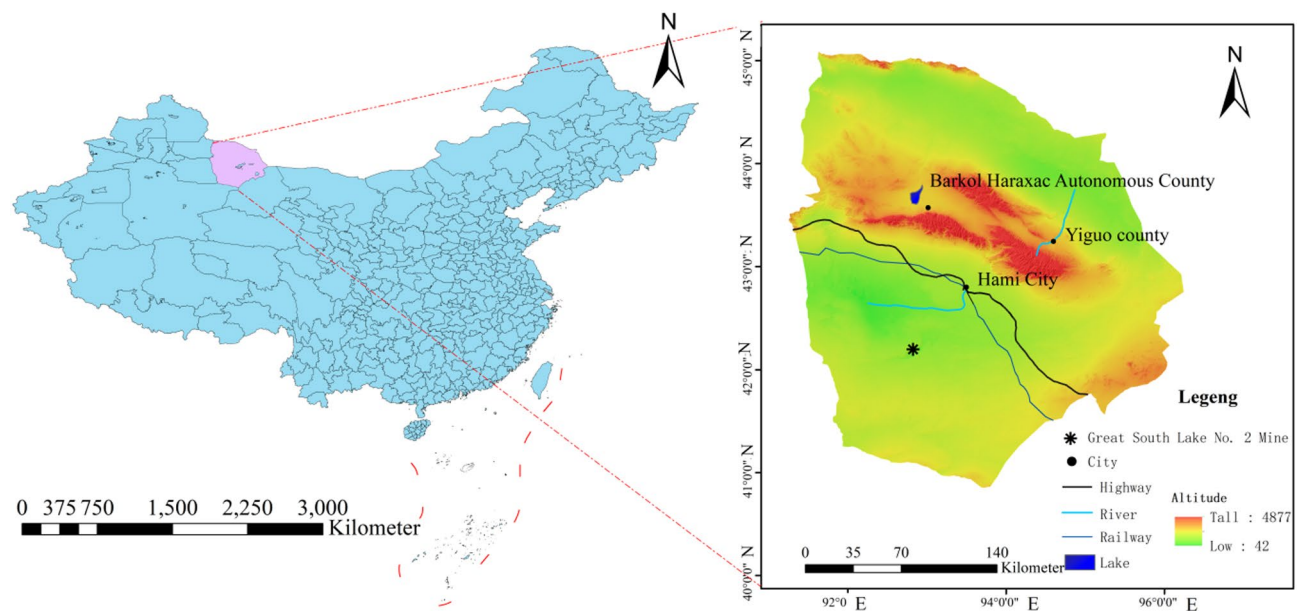


**Fig. 2.** Sampling locations of raw rock at the Dannanhu No.2 Mine. The map in this image was generated by the author using ArcGIS Desktop 10.8 software. You can find information about the software from <http://www.esri.com>

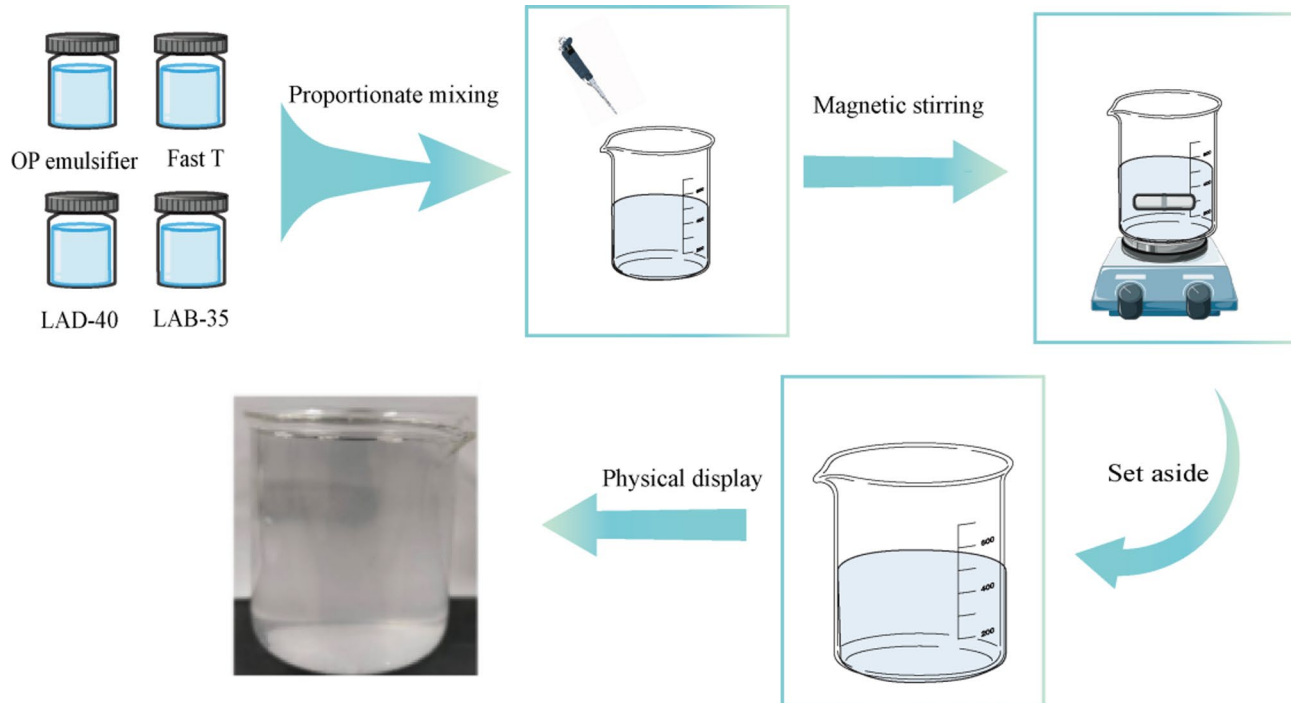


**Fig. 3.** Preparation of water injection wetting agent.

speed of 1000 rpm for approximately 5 min. The remaining water was then added, and the solution was stirred further to ensure complete dissolution and uniform dispersion of the materials. The resulting wetting solution was allowed to stabilize, ensuring that the surfactants were evenly distributed and the solution was ready for subsequent performance testing, as illustrated in Fig. 3.

#### Characterization of raw rock

The physicochemical properties of laminated protolith samples, including chemical functional groups, micromorphology, and contact angle, were analyzed to identify the key factors influencing the wettability of the rock. Samples were collected from the quarrying and loading areas of the Dannahu No. 2 mine in Xinjiang and categorized into six distinct rock layers based on their coloration. The extracted rock specimens underwent initial crushing using a jaw crusher, followed by grinding in a roller ball mill for 8 h. The resultant powdered samples were then placed in a vacuum drying oven at 25 °C and dried to a consistent weight. The prepared rock samples were kept for further analysis.

#### Fourier transform infrared (FT-IR) spectroscopy

A Fourier Transform Infrared Spectrometer (FT-IR) model GXIV5.0.1, manufactured by Perkin Elmer, USA, with a wave number range of 4000–400 cm<sup>-1</sup> was used for the tests. A blank potassium bromide (KBr) film was prepared, and its spectra were recorded to set the baseline for comparison. The rock dust samples were then combined with pure KBr and dried at 105 °C for 2 h in an electric thermostatic blast drying oven. Subsequently, a small quantity of rock dust was mixed with KBr at a 1:1000 ratio using an onyx mortar for grinding. The homogenized mixture was compressed into pellets, which were then analyzed using an FT-IR spectrometer<sup>46,47</sup>.

#### Field emission scanning electron microscope (SEM)

SEM was utilized for morphological analysis. The samples were sieved through a 100-mesh screen and subsequently dried in an oven at 105 °C for 24 h. Following preparation, the samples were coated with a thin layer of gold using ion sputtering under vacuum conditions. The gold-coated samples were then placed in the SEM sample chamber for imaging and analysis. SEM images were acquired at a magnification of 5000 $\times$  to examine the surface morphology in detail.

#### Wetting agent selection

For practical applications, fifteen surfactants were evaluated through experimental analysis. Surface tension and wetting time were used as key parameters to assess their performance.

#### Surface tension measurement

The surface tension of fifteen surfactant solutions was evaluated using the platinum ring method with a JK99C automatic tensiometer. Solutions of the surfactants were prepared at varying concentrations of 0.01%, 0.03%, 0.05%, 0.10%, 0.15%, 0.20%, 0.30%, 0.50%, and 1% by mass. The surface tension values were systematically measured and analyzed to identify surfactants with the lowest surface tension for optimal performance.

S.No.	Considerations			
	OP emulsifier (A)	Fast T (B)	LAD-40 (C)	LAB-35 (D)
1	0.05%	0.05%	0.05%	0.05%
2	0.05%	0.10%	0.10%	0.10%
3	0.05%	0.15%	0.15%	0.15%
4	0.10%	0.05%	0.10%	0.15%
5	0.10%	0.10%	0.15%	0.15%
6	0.10%	0.15%	0.05%	0.10%
7	0.15%	0.05%	0.15%	0.10%
8	0.15%	0.10%	0.05%	0.15%
9	0.15%	0.15%	0.10%	0.05%

**Table 1.** Table of orthogonal experimental design.

Assessment indicators	1	2	3	4	5	6	7	8	9
X	45.053	37.209	36.919	38.736	38.809	35.760	32.465	34.629	38.519
$Y_{\text{upper yellow}}$	28.31	23.28	42.83	109.73	23.86	37.79	16.51	17.85	27.73
$Y_{\text{pure red}}$	58.34	41.39	40.28	112.25	24.07	23.80	26.26	27.18	29.95
$Y_{\text{yellow and white}}$	25.94	23.93	20.46	16.51	23.71	74.94	18.37	27.17	20.37
$Y_{\text{middle}}$	84.86	43.85	45.91	50.47	100.46	38.87	23.54	43.36	75.90
$Y_{\text{pure black}}$	15.61	13.98	20.24	15.53	37.64	19.21	18.24	14.38	17.16
$Y_{\text{lower}}$	17.89	14.50	13.99	41.89	74.19	50.41	16.00	10.89	15.74

**Table 2.** Orthogonal experiment data table. Note: The assessment index X is the measured value of surface tension, mN/m;  $Y_i$  is the measured value of penetration time of six rock formations, s.

#### Penetration time analysis

Six surfactants, including Tween-80, were selected based on the results of the surface tension tests described earlier. These surfactants were evaluated for their wetting efficiency on six distinct types of laminated protolithic dust. Solutions of the surfactants were prepared at mass concentrations of 0.01%, 0.03%, 0.05%, 0.10%, 0.15%, and 0.20%, respectively. The forward penetration test was employed to assess the penetration characteristics of the surfactants. For each test, 2.5 g of rock dust was accurately weighed and placed into a glass tube sealed at one end with medical tape. The tube was tapped lightly 100 times to ensure uniform packing. A pipette was used to add 5 mL of the prepared surfactant solution into the tube, ensuring the solution was introduced within 2 s. The time required for the solution to penetrate 1 cm of the rock dust was recorded for analysis.

#### Orthogonal experiment design

From the various surfactant types, Fast T, OP emulsifier, LAD-40, and LAB-35 were selected as individual components for compounding. The critical micelle concentrations (CMCs) of the individual surfactant 0.05%, 0.10%, and 0.15%, were chosen as the three levels for the orthogonal experiment. These levels were combined with the four surfactants as factors, as outlined in Table 1. The experimental design was constructed using an orthogonal table with four factors and three levels.

A total of nine compound solutions were formulated, leading to 72 experimental groups. The two primary evaluation parameters were surface tension (X) and wetting time (Y). The surface tension of the nine compound solutions and their wetting times in six distinct laminated protolithic dust samples were measured and analyzed, as mentioned in Table 2.

#### Wetting agent comparative experiment

The technical feasibility of the self-developed wetting formulations was evaluated by comparing their performance with laboratory-tested wetting agents. For the comparative analysis, three types of commercially available wetting agents (The main ingredients of the environmentally friendly, polymer-based and conventional types are Sodium fatty alcohol ether sulfate, Polyacrylate and Fatty amine polyoxyethylene ether, respectively) were selected, along with a self-developed formulation. Pure water was used as the control. Experimental conditions, including wetting agent concentration, ambient temperature, and wind speed, were standardized across all tests. The surface tension of the four liquid samples, as well as their wetting times on six distinct types of laminated protolithic dust, were measured. Each test group included three parallel samples, and the average values were calculated for comparison.

#### Modeling of water injection in raw rock

Numerical simulations of water injection into raw rock were conducted using FLUENT, a computational fluid dynamics (CFD) tool within the ANSYS Workbench simulation platform. The numerical simulations in this

article were generated using ANSYS 2022 R2 software used by the authors. You can find information about the software from <https://www.ansys.com/zh-cn/products/ansys-workbench> URL. This platform can simulate a wide range of flow conditions, from incompressible to highly compressible fluids. FLUENT utilizes the finite volume method, supported by fully unstructured meshes, along with gradient-based algorithms for grid nodes and cells. It offers a variety of advanced turbulence models, enabling accurate simulation of inviscid, laminar, turbulent, and seepage flow regimes. For this study, a 3D water injection model was developed based on a mine borehole pre-wetting scheme. The borehole was modeled with a diameter of 1 m and a depth of 1 m, while the computational domain was defined as a square with a side length of 10 m. The resulting simulation and its outcomes were illustrated in Fig. 4.

The 3D model was imported into the Workbench simulation platform with a uniform grid resolution of 0.05 m. The fluid inlet was defined at the wall and the bottom of the borehole, while the boundary conditions encompassed the entire rock calculation domain. For the viscous flow model, the k-epsilon turbulence model was selected, specifically the realizable k-epsilon model, along with the scalable wall function (SWF) for wall treatment. The viscosity of the computational domain was set based on experimental data obtained in previous studies, and the water injection pressure parameters were defined accordingly. The simulation was initialized using the standard initialization method, with a total of 5000 iterations selected for the numerical solution under the specified conditions.

#### Validation of raw rock injection pre-wetting experiments

The experiments were conducted using a rock full stress multi-field coupled triaxial tester. A steady-state method was employed to determine the permeability of the rock samples. To investigate the permeability characteristics of the six distinct layers of flint rock under varying water and water-injected wetting agent pressures, axial and

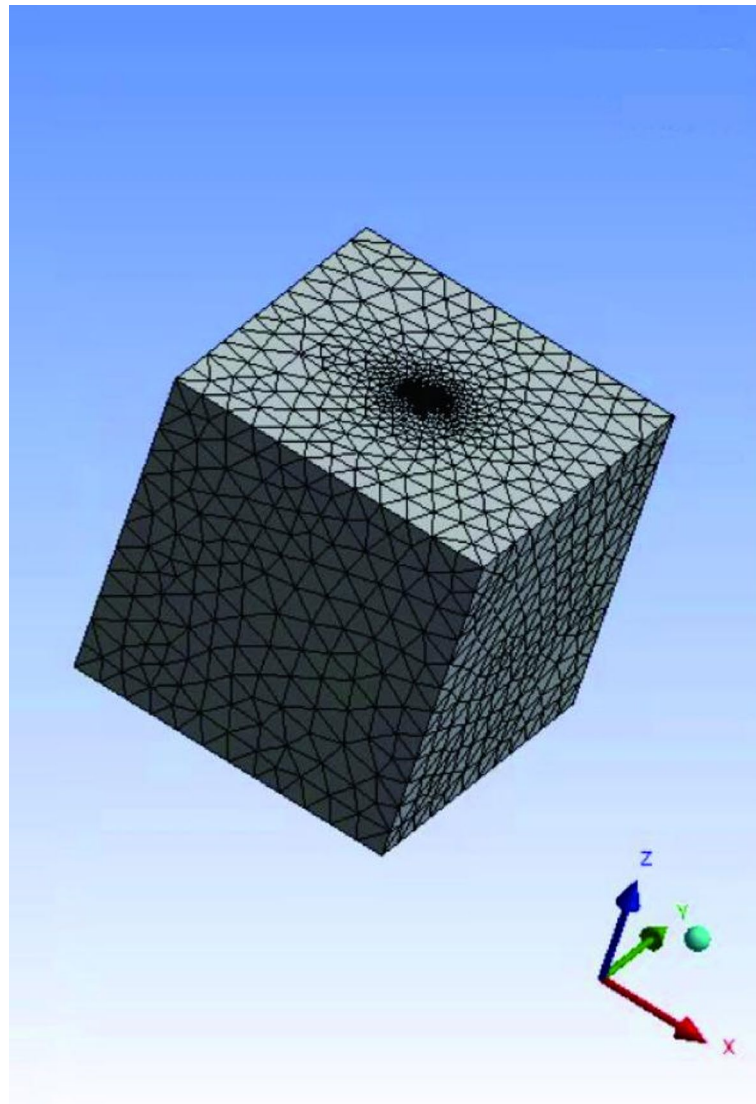


**Fig. 4.** Model diagram of borehole injection.

confining pressures were set to 5 MPa. The permeability pressures were varied at 2, 3, 4, and 5 MPa. During the experiment, the rock samples, having completed the hot and cold cycles, were placed into the triaxial pressure chamber. Axial and confining pressures were applied in a stress-controlled manner, gradually increasing to 7 MPa until stability was achieved. Once stabilized, the permeability pressure was applied. Upon stabilization of the permeability pressure, permeability changes in the rock samples were monitored and recorded automatically by the computer system. Given the slow seepage rate, permeability measurements were taken at 30-minute intervals. When no further changes in permeability were observed, the rock sample was considered fully permeated. The data were then saved, the pressure was released, and the sample was removed, completing the test.

## Experimental results and discussion

### Physical and chemical properties of laminar primary rock dusts

#### FT-IR hydrophilicity analysis of laminated protoliths

The infrared spectra of the six distinct layered rock samples are shown in Fig. 5. From the infrared spectra of the six distinct layered rock samples, it can be seen that absorption peaks appeared near  $1090\text{ cm}^{-1}$  and  $2353\text{ cm}^{-1}$  for different rock samples. These two absorption peaks are the characteristic peaks of the stretching vibration of the C-O group in the alcohol and the characteristic peak of the carboxyl group, respectively, and the presence of oxygen-containing functional groups indicates that there is a certain degree of hydrophilicity in six distinct rock layers. From the figure, it can also be seen that different rock samples contain different numbers of hydrophobic groups, the lower layer, the upper yellow layer, the yellow and white layer and the pure red layer, in addition to the unsaturated telescopic vibration of the aromatic ring near  $1520\text{ cm}^{-1}$ , the characteristic peak of the C-H out-of-plane bending vibration of the aromatic hydrocarbon appeared at  $792\text{ cm}^{-1}$ , indicating that they also have aromatic hydrocarbon substances, which are the root cause of the strong hydrophobicity of the rock samples in six distinct rock layers. These aromatic hydrocarbon substances are the fundamental cause of the strong hydrophobicity of these rock samples<sup>48,49</sup>.

By analysing the infrared spectra, it is found that the six distinct rock samples mainly have three types of groups: aromatic hydrocarbons, aromatic rings and oxygen-containing functional groups. The aromatic hydrocarbon substances and aromatic rings contained on the surface of the rock dust are the fundamental causes of the hydrophobicity of the rock dust. The oxygen-containing groups on the surface of the rock dust maintain a certain degree of hydrophilicity. The difference in the number and type of hydrophobic groups leads to the difference in hydrophobicity, which ultimately leads to the difference in hydrophobicity of the whole rock layer.

#### SEM analysis of six distinct layered Raw rocks

As shown in Fig. 6, SEM image, taken at a magnification of 5000x, revealed significant irregularity in the particle size and shape of the original rock surface. The particles appeared predominantly angular with distinct edges.

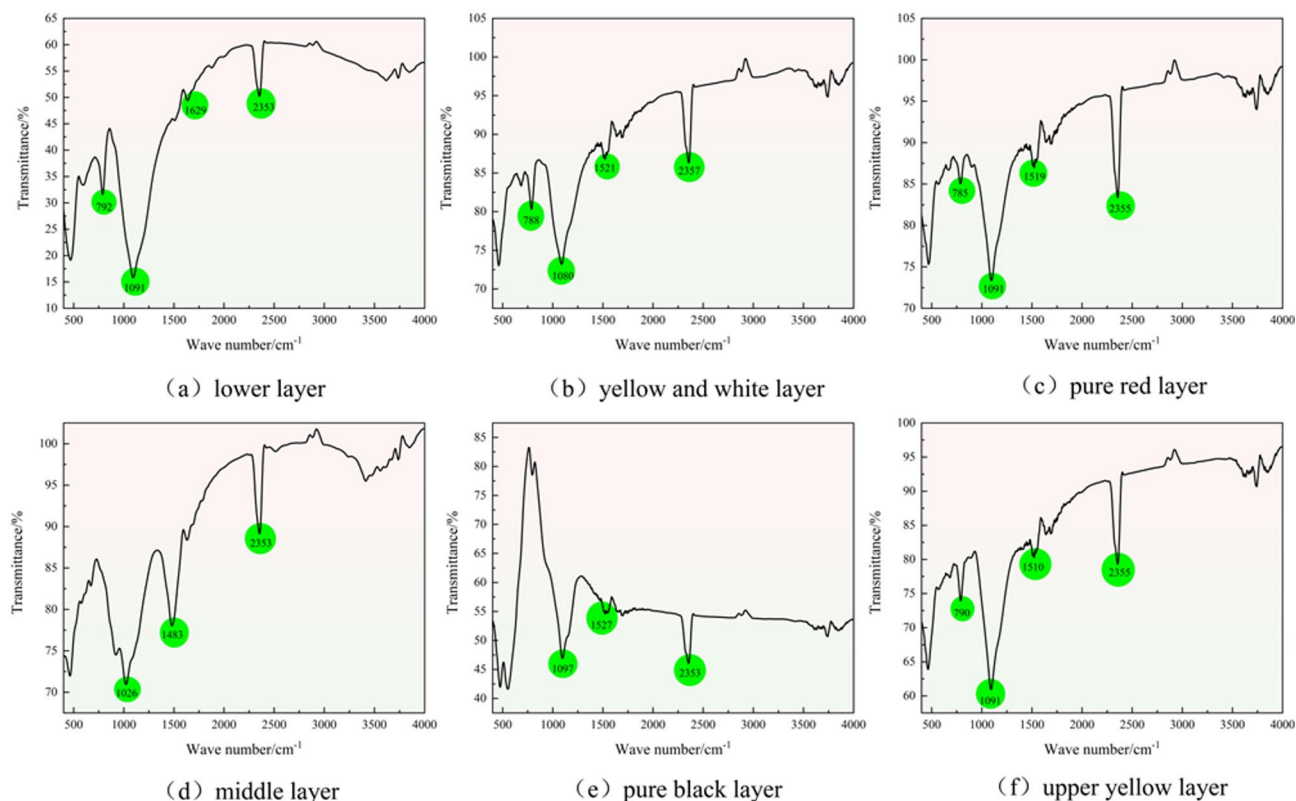


**Fig. 5.** FT-IR spectra of dust from six distinct laminated protolith layers.

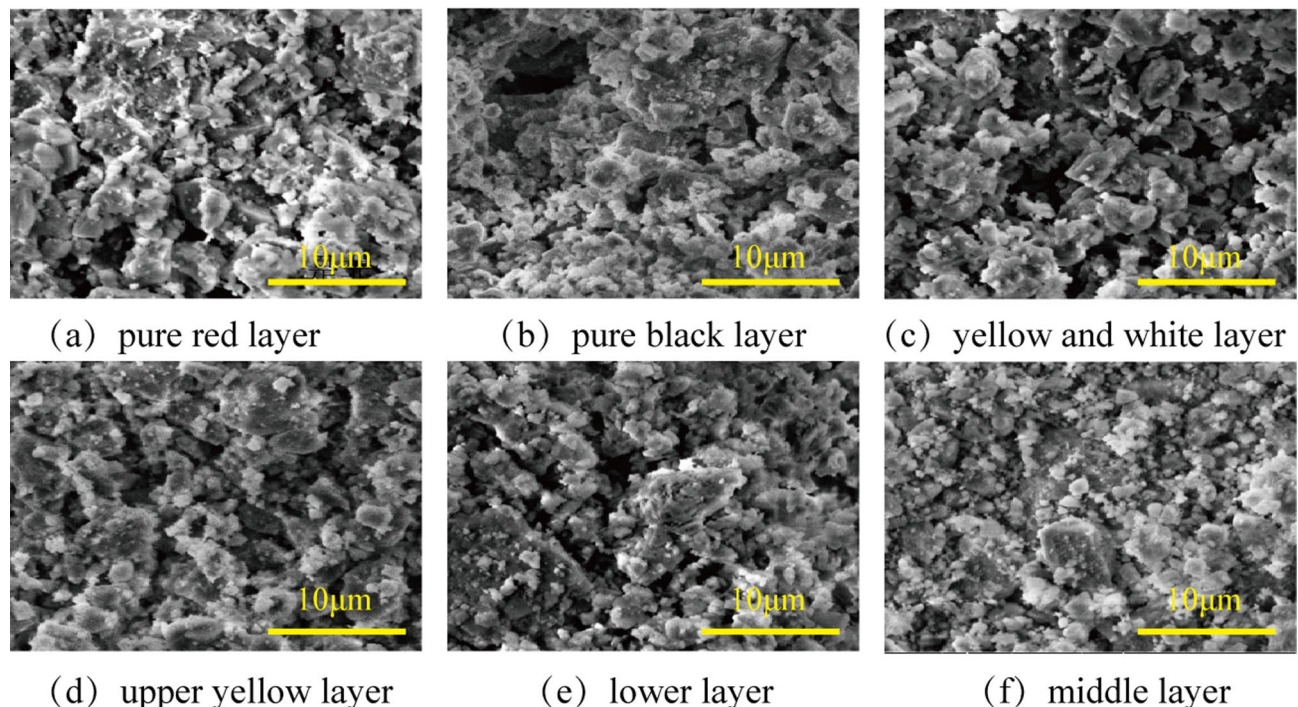


**Fig. 6.** SEM (5000X) of rock samples.

Contact angle/o					
Middle layer	Lower layer	Yellow and white layer	Pure black layer	Pure red layer	Upper yellow layer
85.38	89.5	88.42	87.5	99.38	87.48

**Table 3.** Contact angle measurements of laminated protoliths.

The surface of the rock dust was observed to be highly rough, which hindered the diffusion of the solution across the surface. This roughness contributed to the increased hydrophobicity of the rock dust, making it more challenging to wet.

#### *Contact angle analysis of laminated Raw rock*

The contact angle measurements, presented in Table 3, indicated that the contact angle values for the six distinct layers of rock samples ranged from a maximum of 89.5° to a minimum of 85.38°, with an average value of 87.78°. All measured angles fell within the range of 80° to 90°, indicating that the rock samples exhibited poor wettability.

#### *Wetting agent dust suppression principle*

The core of the dust suppression mechanism is to use surface activity to enhance the affinity of the liquid to the dust, surfactant molecules containing hydrophilic and hydrophobic groups, the hydrophilic end of the hydrophilic end of the water combination, the hydrophobic end of the adsorption on the surface of the dust, greatly reducing the surface tension of water, breaking the exclusion of dust and water, so that the hydrophobic dust (e.g., coal dust, mining dust) is easy to be wetted. The solution with low surface tension quickly spreads into a film on the surface of the dust, penetrates into the interstices of the particles, prompts the dry dust to absorb water and agglomerate, increases the particle size and weight, and reduces the possibility of being lifted up by the airflow. At the same time, the wetting agent molecules strengthen the adhesion between the liquid film and the dust through adsorption to enhance the stability of the agglomeration and to suppress the dust for a long time.

#### **Analysis of wetting agent screening results**

##### *Surface tension test results analysis*

As illustrated in Fig. 7, the surface tension of solutions prepared with the fifteen surfactants decreased significantly with increasing mass fraction. This reduction continued until the critical micelle concentration (CMC) was reached, after which it stabilized. For most of the surfactants, the surface tension leveled off within a mass fraction range of 0.05–0.20%. Specifically, the surface tension of solutions containing Tween-80, OP emulsifier, SDS, Fast T, LAD-40, and LAB-35 was significantly lower than that of pure water (71.82 mN/m). The CMC

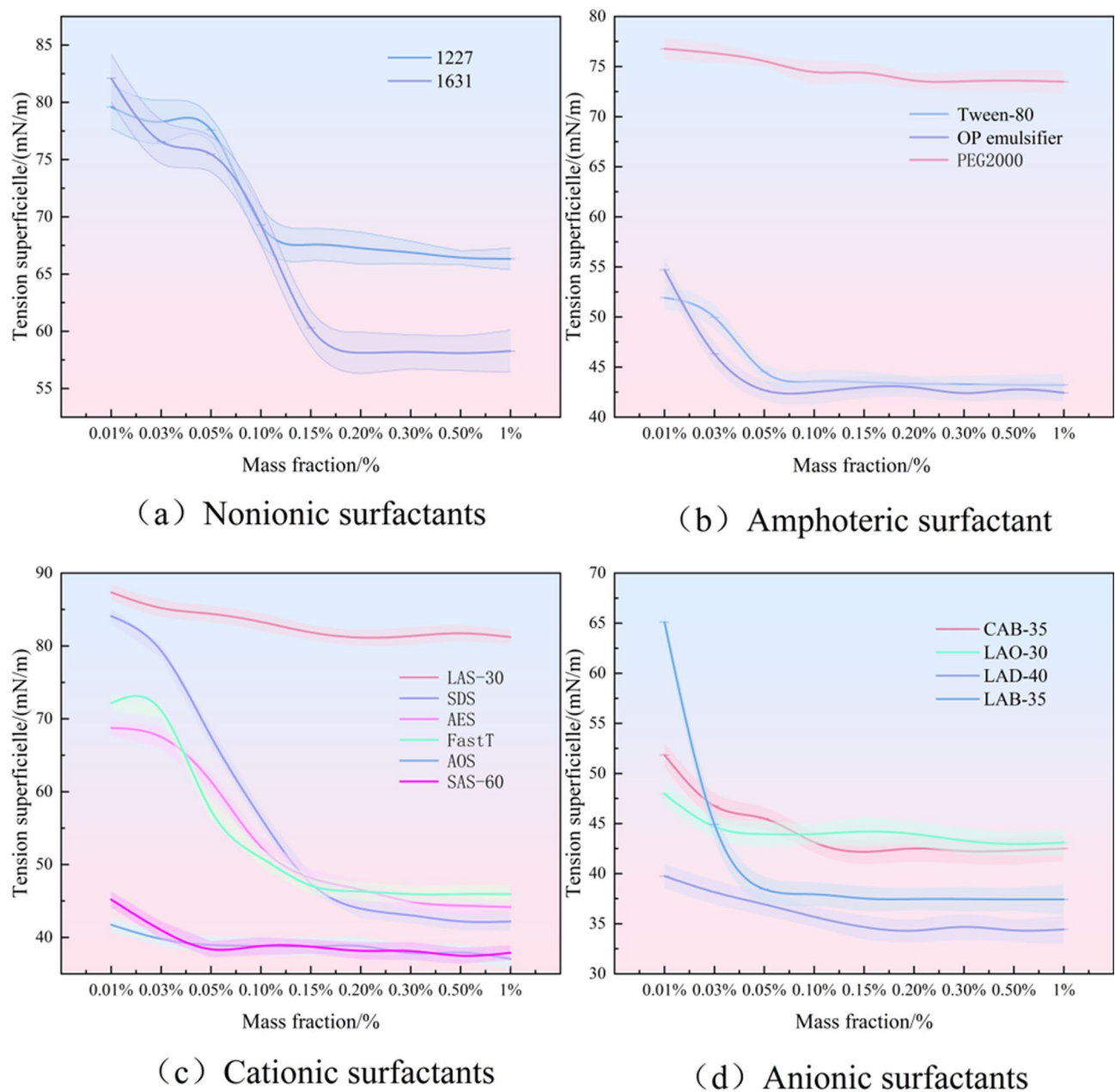


**Fig. 7.** Surface tension versus mass concentration of four surfactants.

values for these six surfactants were found to be 0.10%, 0.20%, 0.05%, 0.10%, 0.05%, and 0.15%, respectively. The ability of these surfactants to reduce the surface tension followed this order: Fast T > OP emulsifier > LAD-40 > LAB-35 > Tween-80. Based on the CMC results, Fast T and OP emulsifier were identified as the most effective surfactants. For the remaining nine surfactants, which exhibited CMC values above 45 mN/m, they were unable to effectively lower the surface tension of water, making their solutions unsuitable for achieving the desired wetting effect. Therefore, the penetration time measurement experiment was not conducted for these surfactants.

#### *Permeation time measurement results analysis*

The permeation time of four surfactants: Tween-80, OP emulsifier, Fast T, and LAB-35 initially decreased and then increased with varying surfactant mass fraction. In contrast, SDS and LAD-40 showed a pattern of increasing, then decreasing, and then increasing again, as shown in Fig. 8. While the penetration rate trend for each surfactant remained largely consistent across different rock samples, notable variations in their permeation performance were observed. The experimental results indicated that the minimum permeation time occurred within a specific range of surfactant mass fractions, corresponding to the maximum penetration rate and optimal permeability. Based on these findings, OP emulsifier, Fast T, LAD-40, and LAB-35 were selected as the candidate

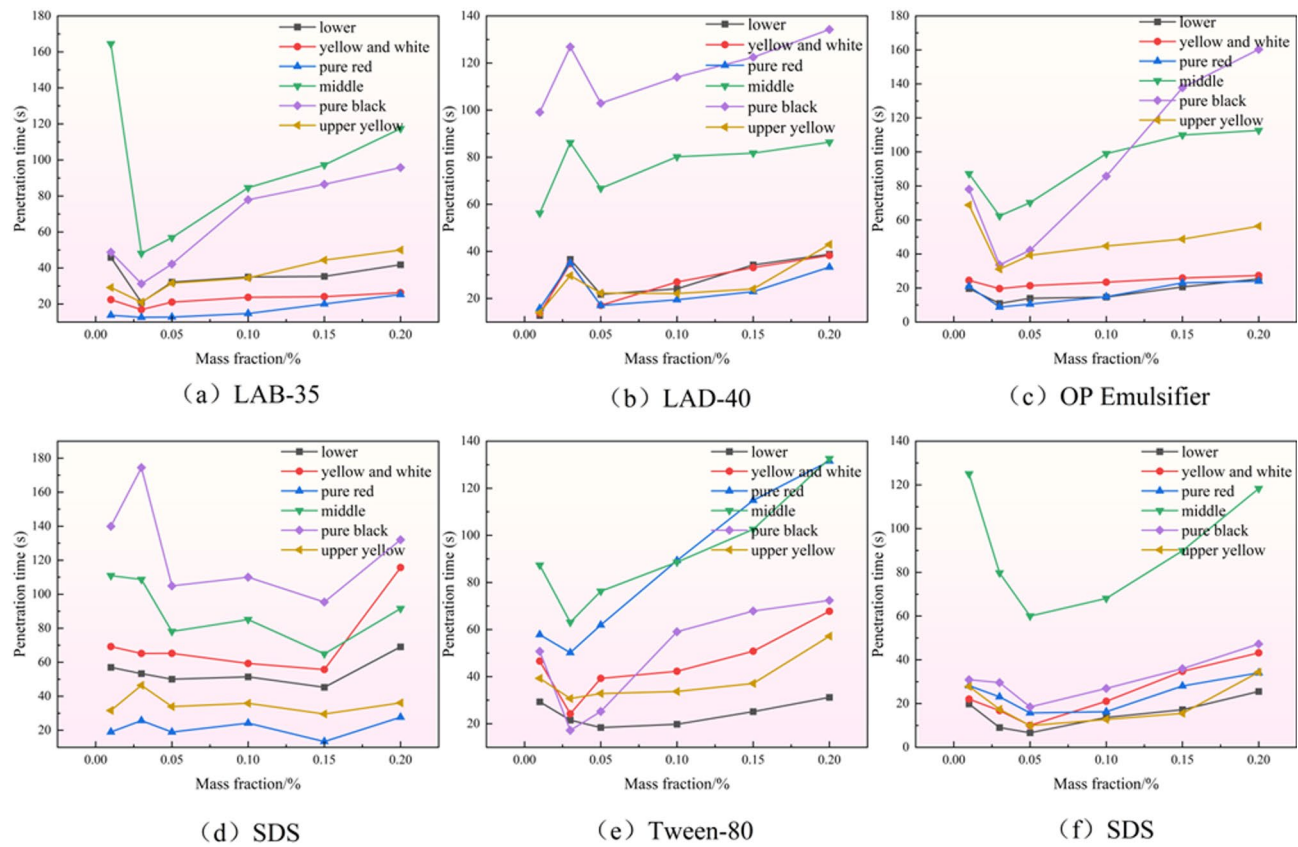


**Fig. 8.** Wetting time of the six surfactants in different rock samples.

surfactants for the orthogonal experiments aimed at formulating the raw rock injection wetting agent for use in the working face.

#### Optimal formulation of water injection wetting agent for laminated protoliths based on orthogonal experiments

The results of the orthogonal experiments were presented in Table 4. Let  $K_1 = X_1 + X_2 + X_3$ ;  $K_2 = X_4 + X_5 + X_6$ ;  $K_3 = X_7 + X_8 + X_9$ . For the surface tension measurements, the experimental indices were calculated as follows: For factor level  $A_1$ , the experimental index:

$$k_1 = K_1/3 = (45.05 + 37.21 + 36.92)/3 = 39.73 \quad (1)$$

For factor level  $A_2$ , the index  $k_2$  was calculated as:

$$k_2 = K_2/3 = (38.74 + 38.81 + 35.76)/3 = 37.77 \quad (2)$$

For factor level  $A_3$ , the index was calculated as

$$k_3 = K_3/3 = (32.46 + 34.63 + 38.52)/3 = 35.20 \quad (3)$$

The orthogonal experimental design ensured that  $A_1$ ,  $A_2$ , and  $A_3$  were conducted under identical conditions, allowing direct comparison of  $k_1$ ,  $k_2$ , and  $k_3$ . The experimental results demonstrated that the variation in  $A_i$  had a direct impact on the outcomes, invalidating the assumption that there was no relationship between the experimental index and surfactant type. Since the surface tension measurement served as the experimental indicator, with smaller  $k_i$  values indicating better performance, factor level  $A_3$  was identified as the optimal level.

Similarly, analysis of the experimental results indicated that  $B_2$ ,  $C_3$ , and  $D_2$  were the superior levels for factors B, C, and D, respectively. The extreme difference  $R_n = \max(k_n) - \min(k_n)$  was calculated to evaluate the influence of various factors on the experimental index. Based on the magnitude of R, the order of influence of the surfactants was determined as  $R(D) > R(A) > R(C) > R(B)$ . This ranking suggests that the LAB-35 surfactant had the most significant impact, followed by the OP emulsifier, LAD-40, and Fast T. Finally, by comparing the  $k_i$  coefficients and R values, the optimal formulation for the water injection wetting agent in open working faces was identified. A lower  $k_i$  coefficient was consistently associated with better performance, guiding the selection of the best parameter combinations for surface tension, contact angle, and wetting time.

Master control indicator		$k_1$	$k_2$	$k_3$	Polar deviation $R$	Formulas
Surface Tension Measurement	A	39.73	37.77	35.2	13.57	$A_3B_2C_3D_2$
	B	38.75	36.88	37.07	5.61	
	C	38.48	38.15	36.06	7.25	
	D	40.79	35.14	36.76	16.95	
Measured wetting time of upper yellow layer rock samples	A	31.47	57.13	20.70	109.29	$A_3B_1C_1D_2$
	B	51.52	21.66	36.12	89.56	
	C	27.98	53.58	27.73	77.54	
	D	26.63	25.86	56.80	92.83	
Measured wetting time of pure red bed rock samples	A	46.67	53.37	27.80	76.73	$A_3B_1C_2D_3$
	B	65.62	30.88	31.34	104.21	
	C	36.44	61.2	30.20	92.98	
	D	37.45	30.48	59.90	88.26	
Measured wetting time of yellow and white layer rock samples	A	23.44	38.39	21.97	49.25	$A_3B_1C_2D_3$
	B	20.27	24.94	38.59	54.95	
	C	42.68	20.27	20.85	67.24	
	D	23.34	39.08	21.38	53.1	
Measured wetting time of middle layer rock samples	A	58.21	63.27	47.6	47.00	$A_3B_1C_2D_3$
	B	52.69	62.56	53.56	26.99	
	C	55.70	56.74	56.64	2.82	
	D	87.07	35.42	46.58	154.96	
Determination of wetting time of rock samples in pure black layer	A	16.61	24.13	16.59	22.6	$A_3B_2C_3D_2$
	B	16.46	22.00	18.87	16.62	
	C	16.40	15.56	25.37	29.45	
	D	23.47	17.14	16.72	20.26	
Measured wetting time of lower layer rock samples	A	15.46	55.50	14.21	123.86	$A_3B_2C_3D_2$
	B	25.26	33.19	26.71	23.8	
	C	26.40	24.04	34.73	32.05	
	D	35.94	26.97	22.26	41.05	

**Table 4.** Measurement of surface tension and wetting time of various rock samples across six distinct rock layers.

From the orthogonal experiments using surface tension as the primary control parameter, the optimal ratio of wetting agent components was identified as  $A_3B_2C_3D_2$ . Forward penetration experiments revealed that the ideal component ratios for six combinations of laminar nodular protolith dust wetting agents varied, specifically:  $A_3B_1C_1D_2$ ,  $A_3B_1C_2D_3$ ,  $A_3B_2C_2D_3$ ,  $A_3B_1C_2D_3$ ,  $A_3B_2C_3D_2$ , and  $A_3B_2C_3D_2$ . For component B, surface tension measurement data indicated that a quality fraction of 0.10% was most effective for reducing surface tension. Wetting time measurements across six rock formations suggested that quality fractions of 0.05% and 0.10% achieved better wetting effects. A comprehensive analysis determined that 0.10% was the optimal quality fraction of component B, enhancing rock sample wettability and improving laminated original rock permeability. Component C, identified as an amphoteric surfactant with superior wetting and penetration capabilities, also demonstrated excellent compatibility. The wetting time results across six rock formations showed an initial increase, followed by a decrease, and then a subsequent increase, leading to the determination of 0.15% as its optimal mass fraction. Similarly, component D, another amphoteric surfactant compatible with cationic, anionic, and nonionic surfactants, exhibited good solubility and consistent performance across various types of surfactants. Its wetting effectiveness on six distinct rock formations identified 0.10% as the optimal mass fraction. Consequently, the orthogonal experiment established the best quality fractions for the self-developed wetting agent for water injection in open-cast coal mines as follows: 0.15% for OP, 0.10% for Fast T, 0.15% for LAD-40, and 0.10% for LAB-35.

#### Analysis of comparative experiment results on wetting agents

Based on the data presented in Fig. 9, the wetting times of liquid samples for six distinct types of laminated protolithic dusts, ranked from shortest to longest, were as follows: self-developed wetting agent < conventional wetting agent < environmentally friendly wetting agent < high-polymer wetting agent < pure water. Similarly, the surface tension of the liquid samples, ranked from lowest to highest, was: self-developed wetting agent < high-polymer wetting agent < conventional wetting agent < pure water. The surface tension of the self-developed wetting agent was measured at 32.47 mN/m. The wetting times for the six distinct types of laminated rock dust were 23.53 s, 10.01 s, 18.38 s, 14.23 s, 26.21 s, and 16.49 s, respectively. These results demonstrated that the self-developed wetting agent achieved the most effective water injection and wetting performance for the six distinct rock layers.

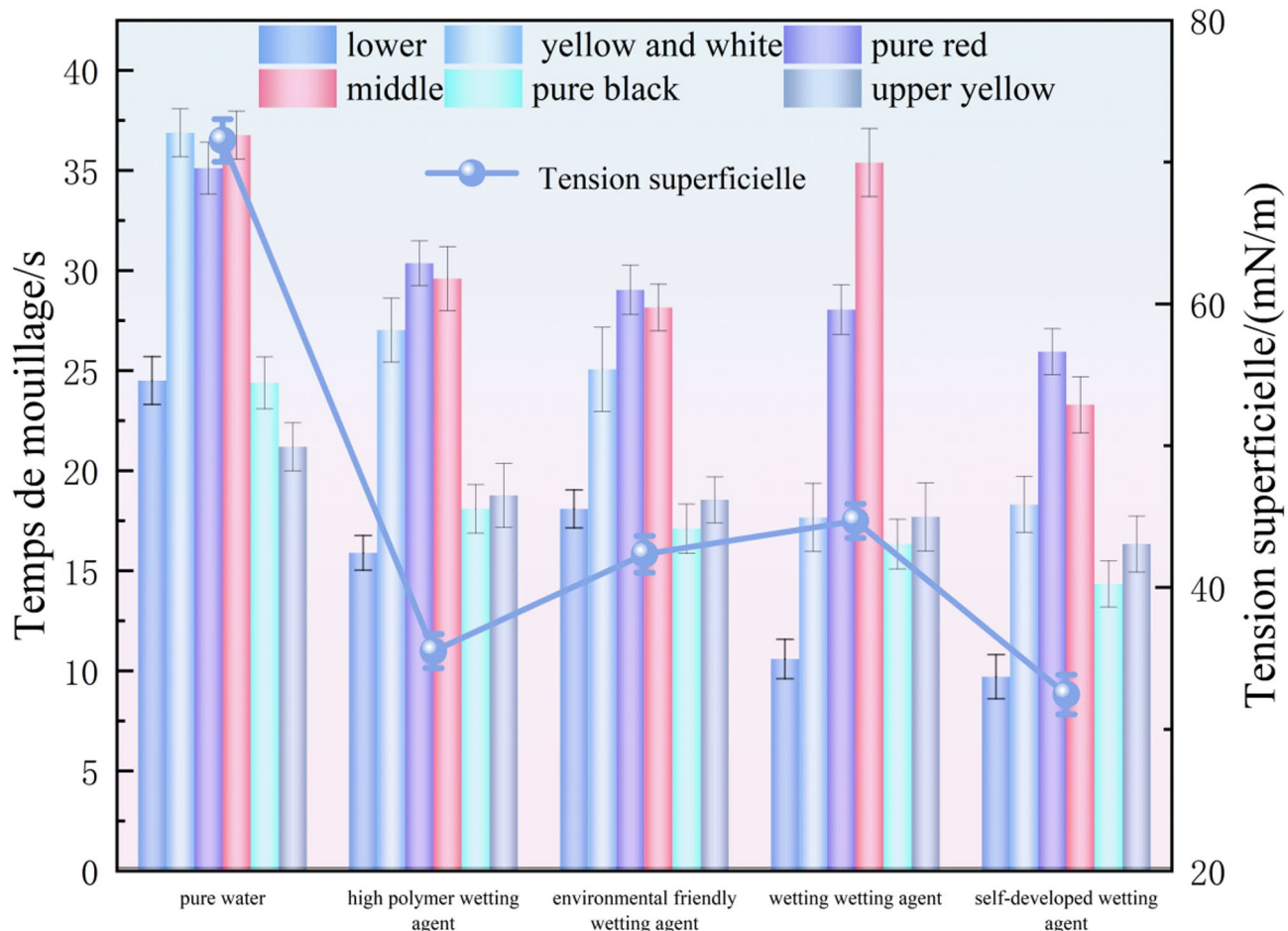


**Fig. 9.** Comparative results among different wetting agents.

This superior performance was attributed to the design of the self-developed wetting agent, which effectively addressed the hydrophobic characteristics of the six distinct layers of laminated rock. By mitigating the overall hydrophobicity of the original rock surface at the working face, the agent minimized hydrophobic resistance and achieved optimal wetting and pre-wetting outcomes.

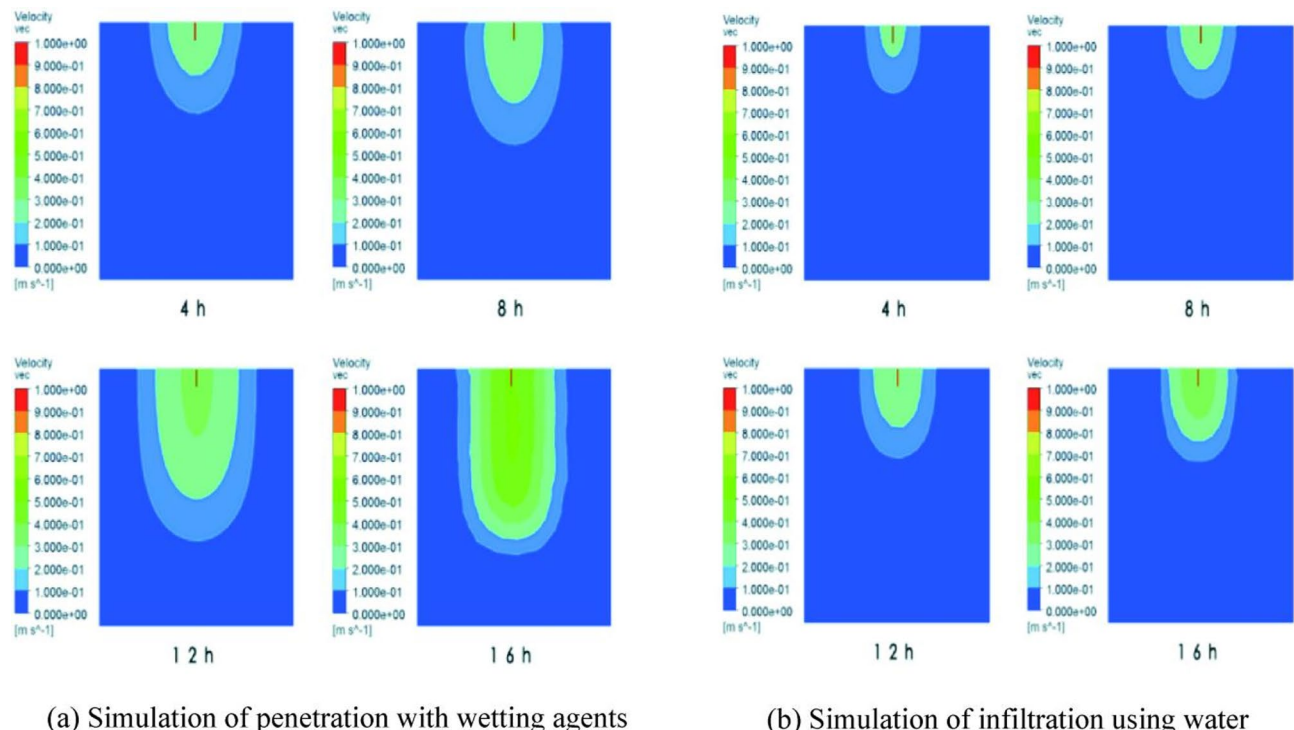
#### Analysis of simulation results for water injection in raw rock of open-pit coal mines

##### *Comparison of simulation results for water injection and wetting agent effects in rock formations*

The numerical infiltration simulation results, illustrated in Fig. 10, showed that during water injection, the water flow initially exhibited rapid longitudinal infiltration under the influence of gravity. Simultaneously, horizontal infiltration occurred due to capillary pressure, with the infiltration velocity gradually decreasing from the interior to the exterior. The observations indicated that the use of a wetting agent in the drilling water significantly improved infiltration compared to using water alone. Specifically, the effective penetration range achieved with the wetting agent was approximately 2–3 times greater than without it, demonstrating an enhanced permeability of the liquid into the rock structure when the water-injection dust-suppressing agent was added. Furthermore, temporal analysis of the images revealed that after 12 h of hydrostatic water injection, the boundary of the infiltration range had largely stabilized. Prolonging water injection beyond this period did not effectively expand the wetted area and would result in resource wastage. Consequently, it was determined that in hydrostatic water injection scenarios, an injection duration of approximately 12 h optimal to maximize efficiency without unnecessary resource consumption.

##### *Simulation of water injection effects at varying pressures*

To investigate the influence of varying water injection pressures on infiltration behavior in a rock mass, simulations were conducted using pressures of 2 MPa, 3 MPa, 4 MPa, and 5 MPa. The simulation results, depicted in Fig. 11, indicated that as the injection pressure increased, the time required to achieve a stable infiltration zone decreased, ranging from 12 h at 2 MPa to 10 h at 3 MPa. However, beyond an injection pressure of 4 MPa, there was no significant reduction in the stabilization time, suggesting a plateau effect. Thus, maintaining the injection pressure at 4 MPa was identified as the optimal condition for efficient water injection, as further increases in pressure do not yield additional benefits in infiltration stabilization.



(a) Simulation of penetration with wetting agents

(b) Simulation of infiltration using water

Fig. 10. Numerical infiltration simulation.

### Analysis of raw rock injection pre-wetting validation experiments

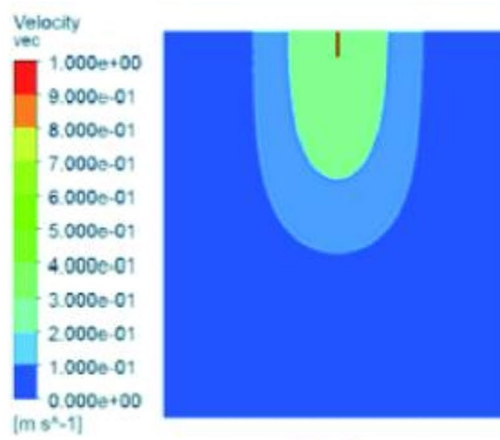
Figure 12 illustrated the variation in seepage coefficients for different rock types under increasing water injection pressures. At an injection pressure of 2.0 MPa, the seepage coefficients were as follows: middle rock,  $5.79 \times 10^{-4}$ ; lower rock,  $5.87 \times 10^{-4}$ ; yellowish-white rock,  $6.22 \times 10^{-4}$ ; pure black rock,  $6.32 \times 10^{-4}$ ; pure reddish rock,  $5.87 \times 10^{-4}$ ; and upper yellow rock,  $6.42 \times 10^{-4}$ . As the water injection pressure increased, the permeability coefficients of six distinct rock layers exhibited a proportional rise. When the injection pressure was increased to 4.0 MPa, the seepage coefficients demonstrate notable increased as follows: middle rock,  $8.24 \times 10^{-4}$ ; lower rock,  $8.32 \times 10^{-4}$ ; yellowish-white rock,  $8.55 \times 10^{-4}$ ; pure black rock,  $8.65 \times 10^{-4}$ ; pure reddish rock,  $7.68 \times 10^{-4}$ ; and upper yellow rock,  $8.45 \times 10^{-4}$ . At this pressure, the wetting effect of the raw rock material reached its optimal state. Beyond this point, further increased in injection pressure yield only marginal improvements in the wetting rate. These experimental findings were consistent with the results obtained through FLUENT numerical simulations, validating the accuracy of the simulation outcomes.

### Conclusion

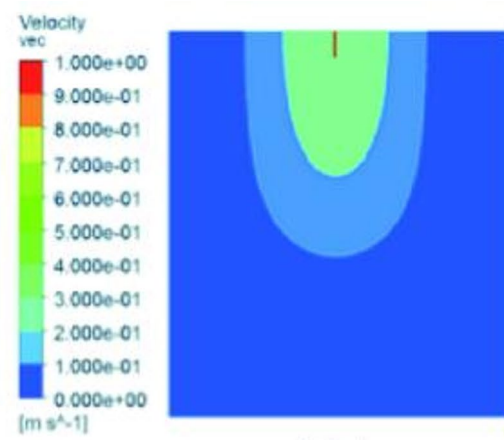
The physicochemical analysis of six bedded protoliths from the Dannahu Mine, Xinjiang, identified aryl rings and aromatic hydrocarbons as primary contributors to their hydrophobicity. Variations in these hydrophobic groups caused significant differences in hydrophilicity, influencing water bypass during injection and pre-wetting, with contact angle experiments validating these findings. Monomer preference and orthogonal experiments determined the optimal wetting agent composition for stratified nodular raw rock as 0.15% OP emulsifier, 0.10% Fast T, 0.15% LAD-40, and 0.10% LAB-35. This formulation improved wettability effectively and consistently within a defined range.

Performance comparisons showed that the self-developed wetting agent was superior to other wetting agents or pure water in reducing the surface tension and wetting the layered raw rock dust, with its self-developed wetting agent having a surface tension of 32.47 mN/m, which minimised the overall raw rock hydrophobicity. In addition, it achieves the optimal wetting and pre-wetting effect for dust reduction. These findings support the use of pre-wetting techniques for dust control in open-cast coal mines.

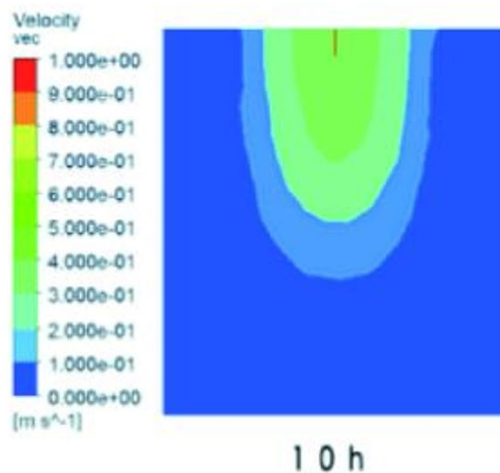
Numerical simulations and verification experiments confirmed that wetting agent solutions enhanced pre-wetting performance over water alone. Increasing injection pressure improved wetting rates, peaking at 4 MPa, beyond which further increases had minimal effect. The results provide a theoretical basis for optimizing water injection pre-wetting in mining operations.



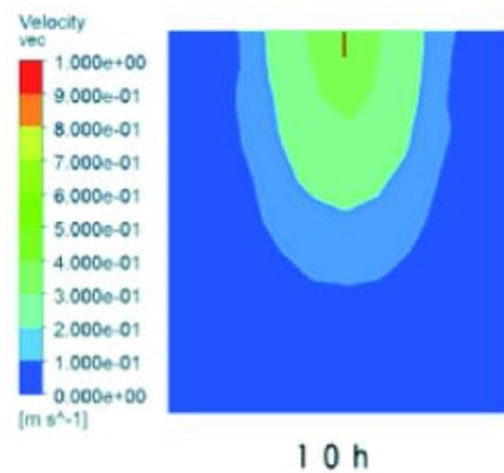
(a) 2 MPa injection pressure



(b) 3 MPa injection pressure



(c) 4 MPa injection pressure



(d) 5 MPa injection pressure

Fig. 11. Infiltration simulation.

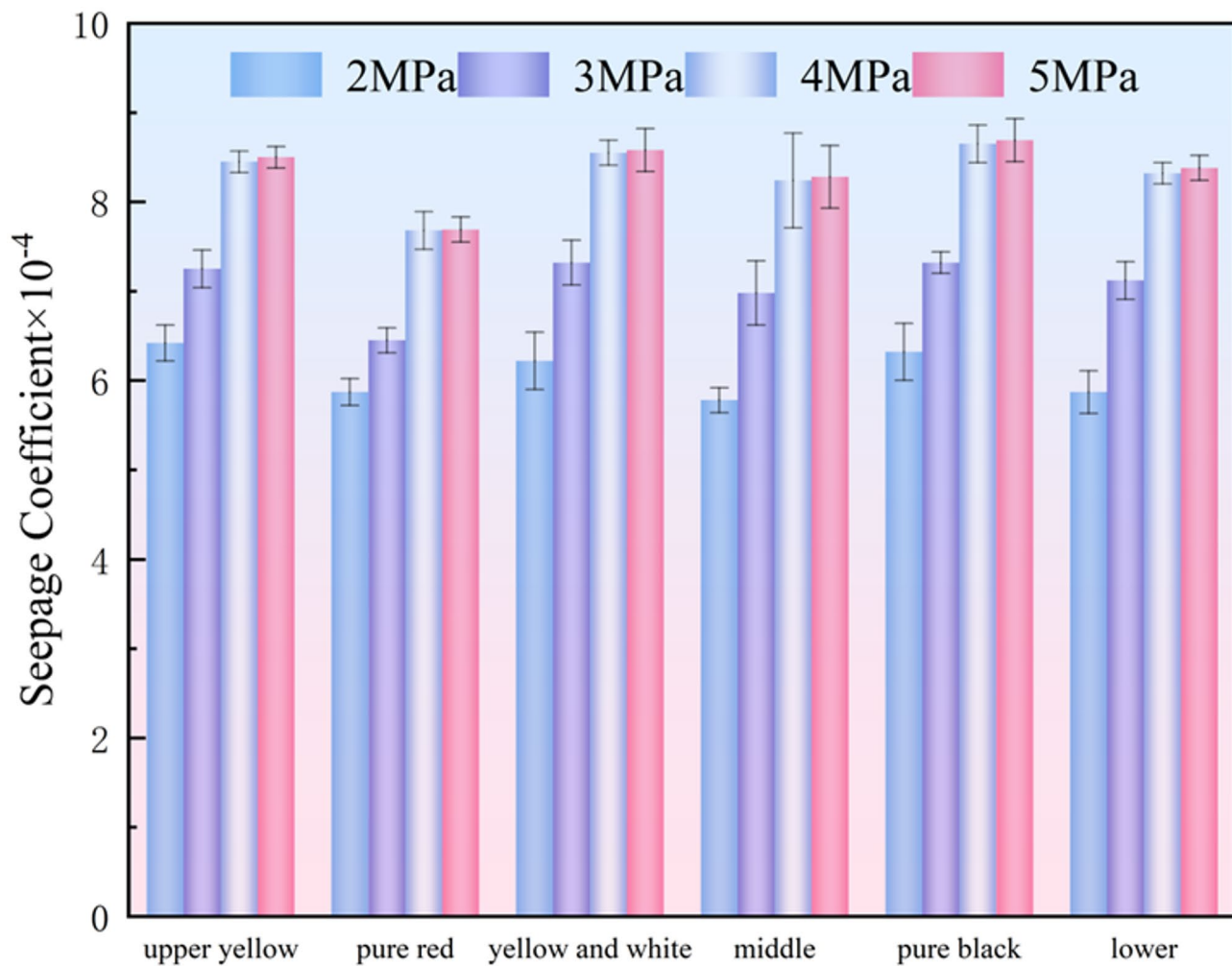


**Fig. 12.** Seepage coefficients of water injection wetting agents at different pressures.

### Data availability

No datasets were generated or analysed during the current study.

Received: 26 February 2025; Accepted: 14 August 2025

Published online: 01 October 2025

### References

1. Lianman, X. et al. Study of effect and mechanism of flame retardation-bursting liability reduction based on chelating water injection wetting agent in coal seam. *Energy Rep.* **8**, 4899–4912 (2022).
2. Leix, Z., Dewen, L. & Shengdong, X. Experimental study on the influence of wetting agent addition on the water adsorption and impact crushing dust generation of coal. *J. Surfactants Deterg.* **5**, 613–619 (2022).
3. Zhen, L., Muyao, Z., He, Y., Dawei, Z. & Kaimeng, Z. Study on the influence of new compound reagents on the functional groups and wettability of coal. *Fuel* **2021**, 302 (2021).
4. Alreshidi, M. et al. Ecological monitoring method and tools for dust suppression during coal transportation and storage. *J. Min. Sci.* **4**, 690–696 (2022).
5. Bingyou, J. et al. Development of an eco-friendly dust suppressant based on modified pectin: experimental and theoretical investigations. *Energy* **289**, 130018 (2024).
6. Conchita, K. et al. The impact of coal mine dust characteristics on pathways to respiratory harm: investigating the pneumoconiotic potency of coals. *Environ. Geochem. Hlth.* **10**, 7363–7388 (2023).
7. Gang, L., Jinhua, H. & Shiqiang, C. A review of dust control/removal methods in metal mines in China. *Powder Technol.* **2023**, 430 (2023).
8. Fangwei, H. et al. Study on the effect of electrolyte on surface tension of surfactant solution and wettability of coal dust, colloid. *Surf. A* **682**, 132929 (2024).
9. Fangwei, H., Jian, L., Yingying, P. & Yue, Z. Exploration of the relationships between the spraying condition and wetting behavior on coal surface of dust suppression droplet: improving the utilization rate. *Geofluids* (2022).
10. Ming, Z. et al. Yue, D. study on the adsorption and dust suppression mechanism of urease-producing bacteria on coal dust. *Powder Technol.* **2022**, 409 (2022).
11. Qiu, B. et al. Molecular simulation and wetting study on the mechanism and capability of hydrophilic surfactants used as spray dust suppressants for dust reduction in coal mines. *Sustainable Chem. Pharm.* **36**, 142 (2023).

12. Wenjin, N. et al. Development and characterization of a high efficiency bio-based rhamnolipid compound dust suppressant for coal dust pollution control. *Environ. Pollut.* **330**, 121792–121792 (2023).
13. Zhou, G. et al. The development and characterization of a novel coagulant for dust suppression in open-cast coal mines, *adsorpt. Sci. Technol.* **1–2**, 608–624 (2018).
14. Xiang-Ming, H. et al. Study on the performance and mechanism of extracellular polymer substances (EPS) in dust suppression. *Powder Technol.* **419**, 142 (2023).
15. Wen, N. et al. Synergistic effect of binary mixture of anionic nonionic surfactant on inhibiting coal dust pollution: experiment and simulation. *J. Environ.* **3**, 856 (2023).
16. Yunfei, S. et al. Physicochemical characteristics and oxidative potential of size-segregated respirable coal mine dust: implications for potentially hazardous agents and health risk assessment. *Int. J. Coal Geol.* **282**, 104433 (2024).
17. Zhao, X. et al. Research and industrial test of anti-freezing and dust suppression agent for truck roads in open-pit mines in inner Mongolia, China. *Processes* **2023**, 12 (2023).
18. Victor, P. M. et al. Pumpkin (*Cucurbita maxima*) seed-derived nitrogen, phosphorus, and sulfur carbon quantum Dot as an inhibitor of corrosion for mild steel in HCl solution. *J. Mater. Res. Technol.* **28**, 2504–2515 (2024).
19. Gan, Z. et al. New type of sawdust-based dust suppressant during tunnelling and underground space: preparation, characterization and engineering application. *Constr. Build. Mater.* **365**, 1452 (2023).
20. Gang, Z. et al. Study on MICP dust suppression technology in open pit coal mine: preparation and mechanism of microbial dust suppression material. *J. Environ.* **343**, 118181–118181 (2023).
21. Huang, Z. et al. Study on the physicochemical characteristics and dust suppression performance of new type chemical dust suppressant for copper mine pavement. *Environ. Sci. Pollut.* **42**, 1–12 (2021).
22. Patrakov, F. Y., Semenova, A. S. & Kharlampenkova, A. Y. Determining the wettability of coal surfaces. *Coke Chem.* **12**, 545–551 (2019).
23. Silvester, S., Lowndes, I. & Hargreaves, D. A computational study of particulate emissions from an open pit quarry under neutral atmospheric conditions. *Atmos. Environ.* **40**, 6415–6424 (2009).
24. Tang, W. & Cai, Q. Dust distribution in open-pit mines based on monitoring data and fluent simulation. *Environ. Monit. Assess.* **11**, 632 (2018).
25. Cheng, W., Ma, Y., Yang, J. & Sun, B. Effects of atomization parameters of dust removal nozzles on the de-dusting results for different dust sources. *IJMST* **6**, 1025–1032 (2016).
26. Zhang, P. et al. Anionic surfactant-activated remediation of Pb, Cd, As contaminated soil by electrochemical technology. *Sci. Total Environ.* **952**, 175889 (2024).
27. Zhao, L., Zhang, L. & Nadeem, M. Z. Synthesis and performance characterization of an efficient environmental-friendly *Sapindus mukorossi* saponins based hybrid coal dust suppressant. *J. Clean. Prod.* **306**, 8596 (2021).
28. Zheng, X., Liu, Y. & Shao, B. Causal analysis of fall accidents in hydraulic engineering based on text mining and decision-making trial and evaluation laboratory and interpretative structural modeling. *Water* **21**, 15 (2023).
29. Jing, D. et al. Novel approach for identifying VOC emission characteristics based on mobile monitoring platform data and deep learning: application of source apportionment in a chemical industrial park. *Helijon* **8**, e29077 (2024).
30. Qingshan, W. et al. Performance optimization and mechanism analysis of applied Enteromorpha-based composite dust suppressant. *Environ. Geochem.* **7**, 4897–4913 (2023).
31. Rongxiao, X., Haiming, Y., Hui, D., Yuxi, Y. & Sen, X. Preparation and properties of modified starch-based low viscosity and high consolidation foam dust suppressant. *J. Hazard.* **452**, 131238–131238 (2023).
32. Zidong, Z. et al. Comparison of the coal dust suppression performance of surfactants using static test and dynamic test. *J. Clean.* **328**, 523 (2021).
33. Zhi, G. et al. Study on the timeliness and maintenance mechanism of dust suppression performance of microbial dust suppressant. *Powder Technol.* **2023**, 426 (2023).
34. Zhilin, X., Tong, X., Liliang, S. & Lianquan, S. Synthesis of cardanol grafted hydrophilic polymers and its mechanism of coal dust Inhibition. *Fuel* **345**, 526 (2023).
35. Wen, N. et al. Study on the combined dust suppression effect of sodium alginate and sodium fatty acid Methyl ester sulfonate. *Adv. Powder Technol.* **11**, 523 (2022).
36. Xiaoliang, Z. et al. A research on dust suppression mechanism and application technology in mining and loading process of burnt rock open pit coal mines. *J. Air Waste Manage.* **12**, 1568–1584 (2021).
37. Zhang, H. et al. Preparation and experimental dust suppression performance characterization of a novel Guar gum-modification-based environmentally-friendly degradable dust suppressant. *Powder Technol.* **399**, 314–325 (2018).
38. Qingsong, Y. D. P. L. & Xin, H. J. H. G. Investigation on coal dust prevention by biomimetic mineralized dust suppressant with polyacrylic acid modifier. *J. Environ.* **2023**, 6 (2023).
39. Wang, H., Wang, C. & Wang, D. The influence of forced ventilation airflow on water spray for dust suppression on heading face in underground coal mine. *Powder Technol.* **320**, 498–510 (2017).
40. Rongxiao, X., Haiming, Y., Hui, D., Yuxi, Y. & Sen, X. Preparation and performance of starch-based cross-linked network structured dust suppression foams for complex Climatic conditions. *Int. J. Biol. Macromol.* **246**, 125645–125645 (2023).
41. Jianying, J. et al. [Invited] optimally configured multi-layer optical fiber plasmonic resonance sensor based on the orthogonal design method, opt.laser. *Technol* **171**, 110413 (2024).
42. Ting, W., Xiaojian, G., Yanlong, L. & Yunhe, L. An orthogonal experimental study on the influence of steam-curing on mechanical properties of foam concrete with fly ash, case. *Stud. Constr. Mater.* **20**, e02665 (2024).
43. Liusheng, X., Miaoqi, B., Yushuai, S., Jinliang, Y. & Xiaofei, W. Transport properties evaluation of pore-scale GDLs for PEMFC using orthogonal design method. *Appl. Energy* **357**, 122445 (2024).
44. Ray, J. et al. A data-driven multiscale model for reactive wetting simulations. *Comput. Fluids* **276**, 106259 (2024).
45. Zhang, C. & Bezuijen, A. Pressure infiltration characteristics of bentonite slurry affected by the salty water: experimental study and mechanistic Understanding. *Acta Geotech.* **11**, 7189–7206 (2024).
46. Haque, J. et al. Triazole-bearing sulfonamide linkage: synthesis, characterization, and investigation as a versatile corrosion inhibitor. *Mol. Struct.* **2024**, 138100 (2024).
47. Subbir, P. D., N. Ullah, H. S., Ravi, K., Ying, H. & Nidhi, T. Fugitive dust suppression in unpaved roads: state of the Art research review. *Sustainability-Basel* **4**, 2399–2399 (2021).
48. Jozanikohan, G. & Abarghooei, M. N. The fourier transform infrared spectroscopy (FTIR) analysis for the clay mineralogy studies in a clastic reservoir. *J. Pet. Explor. Prod. Technol.* **8**, 1–14 (2022).
49. Guoqing, C., Yongsheng, G., Jiaxun, L., Xiangxin, H. & Jianguo, L. Molecular structural evolution during coal oxidation based on in situ FTIR and Raman spectroscopy. *J. Anal. Appl. Pyrol.* **191**, 107209–107209 (2025).

## Acknowledgements

The authors are grateful for Open Project of Collaborative Innovation Center of Mine major Disaster Prevention and Environmental Restoration (CXZX-2024-01) and Scientific Research Project of Liaoning Provincial Department of Education (24-1125).

### Author contributions

Xiaoliang Zhao: Conceptualization, methodology, writing (original draft, review, and editing), Zhaolin Shen: Formal analysis, investigation, data curation, writing (original draft, review, and editing), Bandna Bharti: Writing (review and editing), visualization, supervision, Fangwei Han: Writing (original draft, review, and editing); Shaohui Feng: Writing (original draft, review, and editing), visualization, supervision,

### Funding

Open Project of Collaborative Innovation Center of Mine major Disaster Prevention and Environmental Restoration(CXZX-2024-01). Research on the key technology of anti-freezing and dust suppression for heavy truck pavement in extremely cold open pit mines, Scientific Research Project of Liaoning Provincial Department of Education (24-1125).

### Competing interests

The authors declare no competing interests.

### Additional information

**Correspondence** and requests for materials should be addressed to X.Z.

**Reprints and permissions information** is available at [www.nature.com/reprints](http://www.nature.com/reprints).

**Publisher's note** Springer Nature remains neutral with regard to jurisdictional claims in published maps and institutional affiliations.

**Open Access** This article is licensed under a Creative Commons Attribution-NonCommercial-NoDerivatives 4.0 International License, which permits any non-commercial use, sharing, distribution and reproduction in any medium or format, as long as you give appropriate credit to the original author(s) and the source, provide a link to the Creative Commons licence, and indicate if you modified the licensed material. You do not have permission under this licence to share adapted material derived from this article or parts of it. The images or other third party material in this article are included in the article's Creative Commons licence, unless indicated otherwise in a credit line to the material. If material is not included in the article's Creative Commons licence and your intended use is not permitted by statutory regulation or exceeds the permitted use, you will need to obtain permission directly from the copyright holder. To view a copy of this licence, visit <http://creativecommons.org/licenses/by-nc-nd/4.0/>.

© The Author(s) 2025